Spectrochimica Acta Part A: Molecular and Biomolecular Spectroscopy 240 (2020) 118612

Contents lists available at ScienceDirect

Spectrochimica Acta Part A: Molecular and Biomolecular Spectroscopy

journal homepage: www.elsevier.com/locate/saa

# Spectroscopic and structural studies, thermal characterization, optical proprieties and theoretical investigation of 2-aminobenzimidazolium tetrachlorocobaltate(II)

S. Hassen [a], H. Chebbi [b,c,*], Y. Arfaoui [a], K. Robeyns [d], T. Steenhaut [d], S. Hermans [d], Y. Filinchuk [d]

[a] University of Tunis El Manar, Faculty of Sciences of Tunis, Laboratory of Characterizations, Applications and Modeling of Materials, 2092 El Manar II, Tunis, Tunisia
[b] University of Tunis, Preparatory Institute for Engineering Studies of Tunis, Street Jawaher Lel Nehru, 1089 Montfleury, Tunis, Tunisia
[c] University of Tunis El Manar, Faculty of Sciences of Tunis, Laboratory of Materials, Crystal Chemistry and Applied Thermodynamics, 2092 El Manar II, Tunis, Tunisia
[d] Institute of Condensed Matter and Nanosciences, Université catholique de Louvain place L. Pasteur 1, 1348 Louvain-la-Neuve, Belgium

ARTICLE INFO

*Article history:*
Received 16 March 2020
Received in revised form 24 May 2020
Accepted 10 June 2020
Available online 19 June 2020

*Keywords:*
Hybrid compound
Crystal structure
Hirshfeld Surface (HS)
Spectroscopic measurements
Optical properties
Thermal analysis
DFT calculations

ABSTRACT

In this study we present the crystal structure, spectroscopic and thermal behavior, Hirshfeld surface analysis, and DFT calculations of a new organic-inorganic hybrid compound $(C_7H_8N_3)_2[CoCl_4]$. This compound crystallizes in the centrosymmetric space group $P\bar{1}$. Single-crystal X-ray diffraction analysis indicates that structure consists of a succession of mixed layers formed by organic cations and inorganic anions parallel to the (001) plane and propagate according to the *c*-axis. Layers further are assembled into a 3D supramolecular architecture through N-H···Cl hydrogen bonds and π···π interactions. The peak positions of the experimental PXRD pattern are in agreement with the simulated ones from the crystal structure, indicating phase purity of the title compound. The presence of the different functional groups and the nature of their vibrations were identified by ATR-FTIR and FT-Raman spectroscopies. The tetrahedral environment of $Co^{2+}$ was confirmed by UV–visible spectroscopy, where the spectrum shows three weak absorption bands in the visible range due to d-d electronic transitions $^4A_2(F) \rightarrow {}^4T_2(F)$, $^4A_2(F) \rightarrow {}^4T_1(F)$ and $^4A_2(F) \rightarrow {}^4T_1(P)$ typical of Co(II) coordination compounds. The direct and indirect optical band gap values were determined by Tauc method. The optimized structure and calculated vibrational frequencies were obtained by density functional theory (DFT) using B3LYP functional. TGA and DSC coupled to mass spectrometry (MS) experiments under argon atmosphere in the temperature range (25–950 °C) were carried out in order to determine the thermal stability of the title compound.



## 1. Introduction

In recent years, much attention has been given to a novel class of materials, namely organic– inorganic hybrid materials. This arrangement gives the opportunity of gathering the properties of organic and inorganic compounds at the molecular level. The class hybrid compounds are very wide and features a large set of variable structures, properties, and applications [1]. In particular, the organic-inorganic compounds of general formula $A_2MX_4$, where A is an organic cationic part, M is a divalent transition metal ion and X is a halide anion (Cl, Br, I), has received much attention [2]. Most of these materials exhibit multiple phase transitions attributed to the reorientational dynamics of the substituted amino groups. Such a mechanism of structural phase transitions was classified as "order-disorder" [3]. This is due to the various physical and chemical properties they provide, leading to applications in electrical [4,5], magnetic [6–10], optical [11–13] and antimicrobial [14] fields. These compounds have provided an excellent starting point for the creation of magnetic and semiconducting materials due to their interesting optical properties, and the development of low-cost electronic devices. The structural topology of these materials can be tuned by careful selection of the $MX_4$ tetrahedral anions, the organic cation and some weak interactions such as directional hydrogen bonds, D-H···X (X = Cl, Br, I; and D = N, O etc.) and C-H···π or π···π interactions. These interactions also often play an important role in the construction of these molecular materials. Considering the attractive structural, optical, electrical and catalytic properties of the organic tetrachlorocobaltate(II) [15–17] and the new promising opportunities they may open with regard to the development of useful organic–inorganic hybrid materials [18,19], the present study reports the synthesis of the new 2-aminobenzimidazolium tetrachlorocobaltate(II) compound, structural characterization by single crystal and powder X-ray diffraction, spectroscopic study, optical properties, thermal analysis (TGA/DSC), mass spectrometry (MS) and Hirshfeld surfaces analysis. In addition, a reliable attribution of vibrational bands in the infrared and Raman spectra was done with the aid of density functional theory (DFT) calculations.

* Corresponding author.
*E-mail address:* chebhamouda@yahoo.fr (H. Chebbi).

https://doi.org/10.1016/j.saa.2020.118612
1386-1425/

## 2. Experimental

### 2.1. Materials and measurements

Solvents and reagents were obtained from commercial sources and used as received, $CoCl_2 6H_2O$, 2-aminobenzimidazole and HCl (37%) were obtained from Aldrich. The powder X-ray diffraction pattern was measured at room temperature on the powder diffractometer at the SNBL beamline of the European Synchrotron Radiation Facility (ESRF), Grenoble, France. The wavelength of the incident X-ray was 0.798 Å. ATR-IR spectrum was recorded on a Bruker Alpha spectrometer equipped with a platinum ATR module (diamond crystal) in the 4000–370 $cm^{-1}$ range. Raman scattering spectrum was recorded using a Bruker FT Raman RFS 100/S spectrometer in the frequency range 0–2000 $cm^{-1}$, using a 1064 nm laser. UV–visible spectrum was recorded on an UV-1700 PharmaSpec form Shimadzu in the range of 200–800 nm in an absolute ethanol solution. The thermogravimetric (TGA) and differential scanning calorimetry (DSC) measurements under argon atmosphere (25–950 °C) were carried out using a Netzsch STA 449 F3 Jupiter TGA/DSC device equipped with a stainless steel oven housed in an argon-filled glovebox and coupled to a Netzsch QMS 403 D Aëolos mass spectrometer. 9.65 mg of compound was used for these measurements. The measurements were performed under an argon flow of 100 mL.$min^{-1}$ at a heating rate of 5 °C.$min^{-1}$.

### 2.2. Synthesis of $(C_7H_8N_3)_2[CoCl_4]$

The organic-inorganic hybrid compound was prepared by slow evaporation according to the following chemical equation:

$$2\ C_7H_7N_3 + 2\ HCl \rightarrow 2\ (C_7H_8N_3)Cl \quad (1)$$

$$2\ (C_7H_8N_3)cl + CoCl_2 \rightarrow (C_7H_8N_3)_2[CoCl_4] \quad (2)$$

The first step was the preparation of 2-aminobenzimidazolium chloride $(C_7H_8N_3)Cl$ ($(C_7H_8N_3)^+$, $Cl^-$) that was formed by the addition of an aqueous solution of HCl (37%) to 2-aminobenzimidazole ($C_7H_7N_3$) (2 mmol, 0.270 g) dissolved in 6 mL of ethanol. The added acid quantity has an important role in the reaction product; in this case the pH was adjusted to 5.6. The next step was the formation of the desired compound, when the obtained solution in the first step was added to an aqueous solution (5 mL) of $CoCl_2 6H_2O$ (1 mmol, 0.238 g). The resulting solution was stirred for 1 h and subsequently was left at room temperature. After 9 days, when the solution was evaporated until dryness, blue crystals were obtained. Single crystals were selected and studied by X-ray diffraction analysis, thermal and spectroscopic measurements.

### 2.3. X-ray crystallography

Single crystal X-ray diffraction intensity data were collected at 298 (2) K with Enraf-Nonius CAD4 automatic four-circle instrument equipped with graphite monochromator using Mo $K_\alpha$ radiation ($\lambda$ = 0.71073 Å). Unit-cell parameters were determined by least-squares treatment of the setting angles of 25 reflections in the range (10.73°–15.72°). The crystal structure has been solved in the triclinic system, space group $P\bar{1}$ according to the automated search for space group available in WINGX [20]. The structure was solved with direct methods using SHELXS-97 [21], and refined by a full-matrix least squares technique on $F^2$ with SHELXL-2014/7 [22]. All Hydrogen atoms of the protonated 2-aminobenzimidazolium were positioned geometrically and refined using the riding model [N—H is set to 0.86 Å using $U_{iso}(H) = 1.2\ U_{eq}$ (N) and C–H = 0,93 Å with $U_{iso}(H) = 1.2\ U_{eq}(C)$]. Selected crystallographic data and experimental details are presented in Table 1. Specified hydrogen bonds and selected bond lengths and angles are listed in Tables 2 and 3, respectively.

**Table 1**
Crystallographic data for $(C_7H_8N_3)_2[CoCl_4]$.

| *Chemical formula* | *$(C_7H_8N_3)_2[CoCl_4]$* |
|---|---|
| *Formula weight (g $mol^{-1}$)* | *469.06* |
| *Temperature (K)* | *298* |
| *Crystal system* | *Triclinic* |
| *Space group* | *$P\bar{1}$* |
| *a (Å)* | *7.947 (2)* |
| *b (Å)* | *8.787 (2)* |
| *c (Å)* | *14.293 (2)* |
| *α (°)* | *74.90 (3)* |
| *β (°)* | *86.86 (3)* |
| *γ (°)* | *79.67 (3)* |
| *V ($Å^3$)* | *947.9 (3)* |
| *Z* | *2* |
| *Density calculated (Mg $m^{-3}$)* | *1.643* |
| *Absorption coefficient ($mm^{-1}$)* | *1.48* |
| *F(000)* | *474* |
| *Range for data collection* | *$\theta_{min} = 2.4°$, $\theta_{max} = 27.1°$* |
| *Reflections collected - Independent* | *4531-4159* |
| *$R_{int} - R_1$ [$I > 2\sigma(I)$]-$wR_2$* | *0.030-0.034-0.091* |
| *S(GOF)* | *1.06* |

### 2.4. Theoretical methods

The geometry optimization of the structure was carried out from the structure obtained by single crystal determination. The structure was optimized with the DFT method using the Gaussian 09 program [23]. The calculations were performed using the B3LYP functional and 6-311+G(2d,2p) basis set for H, C, N, Cl and LANL2DZ for Co [24,25]. Vibrational frequency calculations were then performed at the same level of theory of the optimized geometries to confirm that there are no imaginary frequencies. The computed vibrational frequencies were achieved using an appropriate scaling factor of 0.967. The Hirshfeld surfaces and the associated 2D fingerprint plots were calculated using Crystal Explorer 3.1 [26].

## 3. Results and discussion

### 3.1. Crystal structure

The title compound crystallizes in the centrosymmetric space group $P\bar{1}$ of triclinic system. The asymmetric unit was formed by one tetrachlorocobaltate anion $[CoCl_4]^{2-}$ and two protonated 2-aminobenzimidazolium $(C_7H_8N_3)^+$ organic cations (Fig. 1). The geometry of the $[CoCl_4]^{2-}$ anion is characterized by a range of Co—Cl bond lengths from 2.285 (7) to 2.292 (8) Å and Cl-Co-Cl angles varying from 104.9 (3) to 113.7 (3)°, building a slightly distorted tetrahedron. These data are in agreement with those found in related compounds [27,28]. The calculated average values of the distortion indices as described by Baur [29] corresponding to the different lengths and angles

**Table 2**
Specified hydrogen bonds (Å, °) for $(C_7H_8N_3)_2[CoCl_4]$.

| D-H…A | D-H (Å) | H...A (Å) | D...A (Å) | <(DHA)> (°) |
|---|---|---|---|---|
| N1-H1A···Cl2$^{i}$ | 0.860(1) | 2.711(2) | 3.409(3) | 139.18(4) |
| N2-H2A···Cl4 | 0.860(1) | 2.397(2) | 3.227(3) | 162.34(4) |
| N3-H3A···Cl3$^{ii}$ | 0.860(1) | 2.444(2) | 3.261(3) | 158.76(4) |
| N3-H3B···Cl2$^{iii}$ | 0.860(1) | 2.695(2) | 3.368(4) | 136.08(4) |
| N4-H4A···Cl1$^{ii}$ | 0.860(1) | 2.762(2) | 3.408(2) | 133.09(4) |
| N4-H4A···Cl3$^{iv}$ | 0.860(1) | 2.793(3) | 3.397(2) | 128.61(4) |
| N5-H5A···Cl1 | 0.860(1) | 2.451(3) | 3.299(3) | 169.17(4) |
| N6-H6A··· Cl3$^{ii}$ | 0.860(1) | 2.673(2) | 3.327(3) | 133.92(4) |
| N6-H6B···Cl4 | 0.860(1) | 2.413(2) | 3.248(3) | 163.87(4) |

Symmetry codes: (i) -x + 1, −y + 1, −z + 2; (ii) x-1, y, z; (iii) x-1, y + 1, z; (iv) -x + 1, −y + 1, −z + 1.

**Table 3**
Selected bond lengths and angles for the studied compound.

| Bond lengths (Å) | Experimental | Theoretical | Angles(°) | Experimental | Theoretical |
|---|---|---|---|---|---|
| Co-Cl4 | 2.285 (7) | 2.277 | Cl4-Co-Cl1 | 107.9 (3) | 107.8 |
| Co-Cl1 | 2.286 (8) | 2.285 | Cl4-Co-Cl2 | 107.9 (3) | 107.8 |
| Co-Cl2 | 2.292(8) | 2.291 | Cl1-Co-Cl2 | 113.7 (3) | 113.6 |
| Co-Cl3 | 2.292 (8) | 2.292 | Cl4-Co-Cl3 | 109.5 (3) | 109.4 |
| N1-C7 | 1.344 (3) | 1.343 | Cl1-Co-Cl3 | 104.9 (3) | 104.7 |
| N1-C6 | 1.401 (3) | 1.400 | Cl2-Co-Cl3 | 112.7 (3) | 112.6 |
| N2-C7 | 1.342 (3) | 1.342 | C7-N1-C6 | 109.5 (2) | 109.4 |
| N2-C1 | 1.400 (4) | 1.399 | C7-N2-C1 | 109.4 (2) | 109.3 |
| N3-C7 | 1.322 (4) | 1.320 | C14-N4-C8 | 109.2 (2) | 109.3 |
| N4-C14 | 1.341 (3) | 1.341 | C14-N5-C13 | 109.3 (2) | 109.1 |
| N4-C8 | 1.398 (3) | 1.396 | C2-C1-C6 | 121.4 (3) | 120.9 |
| N5-C14 | 1.342 (3) | 1.341 | C2-C1-N2 | 132.1 (3) | 132.3 |
| N5-C13 | 1.401 (3) | 1.400 | C6-C1-N2 | 106.5 (2) | 106.4 |
| N6-C14 | 1.319 (3) | 1.318 | C1-C2-C3 | 116.6 (3) | 116.5 |
| C1-C2 | 1.383 (4) | 1.382 | C2-C3-C4 | 121.7 (3) | 121.6 |
| C1-C6 | 1.389 (4) | 1.389 | C5-C4-C3 | 121.4 (3) | 121.2 |
| C2-C3 | 1.390 (5) | 1.389 | C6-C5-C4 | 116.8 (3) | 116.9 |
| C3-C4 | 1.391 (5) | 1.389 | C5-C6-C1 | 122.2 (3) | 122.2 |
| C4-C5 | 1.383 (4) | 1.384 | C5-C6-N1 | 131.6 (3) | 131.5 |
| C5-C6 | 1.376 (4) | 1.374 | C1-C6-N1 | 106.2 (2) | 105.9 |
| C8-C9 | 1.385 (4) | 1.384 | N3-C7-N2 | 126.7 (3) | 125.9 |
| C8-C13 | 1.390 (4) | 1.379 | N3-C7-N1 | 124.9 (2) | 124.7 |
| C9-C10 | 1.379 (5) | 1.378 | N2-C7-N1 | 108.4 (2) | 108.4 |
| C10-C11 | 1.383 (5) | 1.382 | C9-C8-C13 | 121.5 (3) | 121.3 |
| C11-C12 | 1.395 (5) | 1.393 | C9-C8-N4 | 131.9 (3) | 131.8 |
| C12-C13 | 1.379 (4) | 1.380 | C13-C8-N4 | 106.6 (2) | 106.5 |
| | | | C10-C9-C8 | 116.5 (3) | 116.4 |
| | | | C9-C10-C11 | 122.2 (3) | 122.1 |
| | | | C10-C11-C12 | 121.5 (3) | 120.9 |
| | | | C13-C12-C11 | 116.2 (3) | 116.1 |
| | | | N6-C14-N4 | 125.6 (2) | 125.5 |
| | | | N6-C14-N5 | 125.7 (2) | 125.6 |
| | | | N4-C14-N5 | 108.7 (2) | 108.2 |
| | | | C12-C13-C8 | 122.1 (3) | 122.9 |
| | | | C12-C13-N5 | 131.6 (3) | 131.4 |
| | | | C8-C13-N5 | 106.2 (2) | 106.5 |

in the $CoCl_4$ tetrahedron, DI (Co—Cl) = 0.0015 and DI (Cl-Co-Cl) = 0.0226, show a slight distortion of the tetrahedron.

In the crystal structure, the $[CoCl_4]^{2-}$ tetrahedron and the two protonated 2-aminobenzimidazolium $(C_7H_8N_3)^+$ organic cations are interconnected by intermolecular N2-H2A···Cl4, N5-H5A···Cl1 and N6-H6B···Cl4 hydrogen bonds. The organic-inorganic parts are interconnected by intermolecular N3-H3A···$Cl3^{ii}$, N6-H6A···$Cl3^{ii}$ and N4-H4A···$Cl1^{ii}$ hydrogen bonds, into 1D undulating chains running parallel to the [100] direction of the unit cell, forming graphs set motifs of the types $R_4^2(10)$ and $R_2^2(8)$ [30,31] (Fig. 2). Chains further grow into 2D layers packed along the *c*-axis of the unit cell mediated by N3-H3B···$Cl2^{iii}$ and N1-H1A···$Cl2^{i}$ hydrogen bonds, forming a graph set motif of the type $R_2^1(6)$ (Fig. 3) [32]. These mixed layers formed by organic cations and inorganic anions are parallel to the (001) plane and propagate according to the *c*-axis (Fig. 3). These supramolecular layers are interconnected to adjacent layers via N4-H4A···$Cl3^{iv}$ hydrogen bonds and π···π stacking interactions (Fig. 4), around the inversion center, with centroid-centroid Cg-Cg = 3.49(1) Å [33] forming a 3D supramolecular architecture (Table 2, Fig. 5).

### 3.2. Geometry optimization

The geometry optimization of the title compound was carried out by density functional theory (DFT) using B3LYP functional and 6-311+G (2d,2p) basis set for H, C, N, Cl and LANL2DZ for Co. The obtained optimized geometry of the molecular structure and the X-ray diffraction

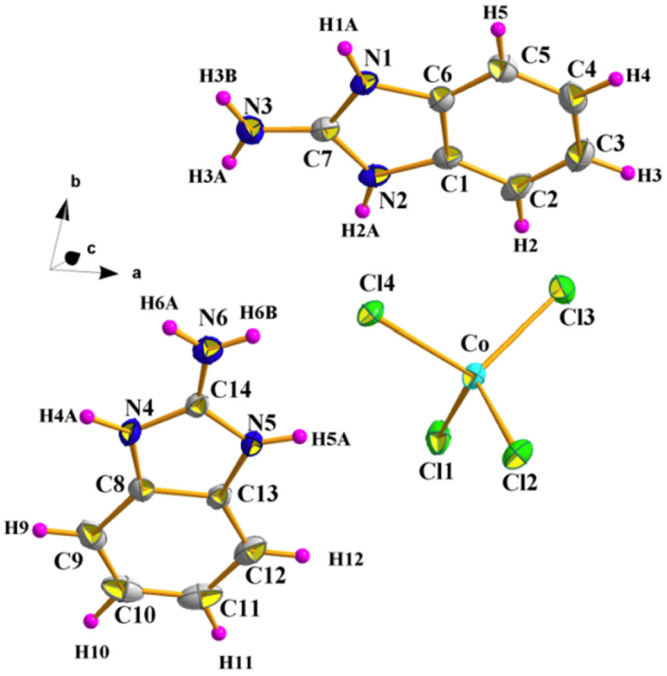


**Fig. 1.** The asymmetric unit of $(C_7H_8N_3)_2[CoCl_4]$, with displacement ellipsoids drawn at the 30% probability level.

structure show an excellent agreement between the experimental and calculated data (Table 3, Fig. 6).

### 3.3. Hirshfeld surface analysis

Hirshfeld surfaces analysis plays a unique role in exposing valuable information on the inter- and intra-molecular interactions close to Van der Waals radii between nearest neighbors. The two cases of molecular Hirshfeld surface $d_{norm}$ for the title compound are illustrated in Fig. 7 and mapped over $d_{norm}$ ranges −0.5013 to 1.3569 Å in case 1 (representing the Hirshfeld surface of the anionic part $[CoCl_4]^{2-}$ with one of the cationic fragment $(C_7H_8N_3)^+$) and − 0.5713 to 1.4769 Å in case 2 (representing the Hirshfeld surface of the anionic part $[CoCl_4]^{2-}$ with the other cationic fragment $(C_7H_8N_3)^+$). The $d_{norm}$ values are represented on the Hirshfeld surface by using red-blue-white coloring. The red regions correspond to negative $d_{norm}$ values for which the intermolecular contacts are shorter than the Van der Waals separations and are representative of significant hydrogen bonding contacts. The blue regions correspond to positive $d_{norm}$ values where the intermolecular contacts are longer than the van der Waals separations and the white areas correspond to intermolecular contacts near the van der Waals separations and $d_{norm}$ values near zero. The 2D fingerprint plots reveal that the H…Cl/Cl…H inter- and intramolecular interactions which involve the N-H···Cl hydrogen bonding is the most significant contribution to the total Hirshfeld surface, comprising 53.3% (case 1) and 54.8% (case 2) of the total number of contacts. The H…H interactions contacts contribute 21.7% (case 1) and 19.9% (case 2) to the total Hirshfeld surface and arises as broad spikes in the fingerprint plot. Furthermore, the C…H/H…C contacts contribute 12.6% (case 1) and 7.7% (case 2). Then the N…H/H…N contacts contribute 3.2% (case 1) and 4.8% (case 2) of the total Hirshfeld surface (Fig. 7). The Hirshfeld surface analysis shows the existence of other weak. These results are in good agreement with the structural study where the structure is dominated by N-H…Cl interactions in the crystal.

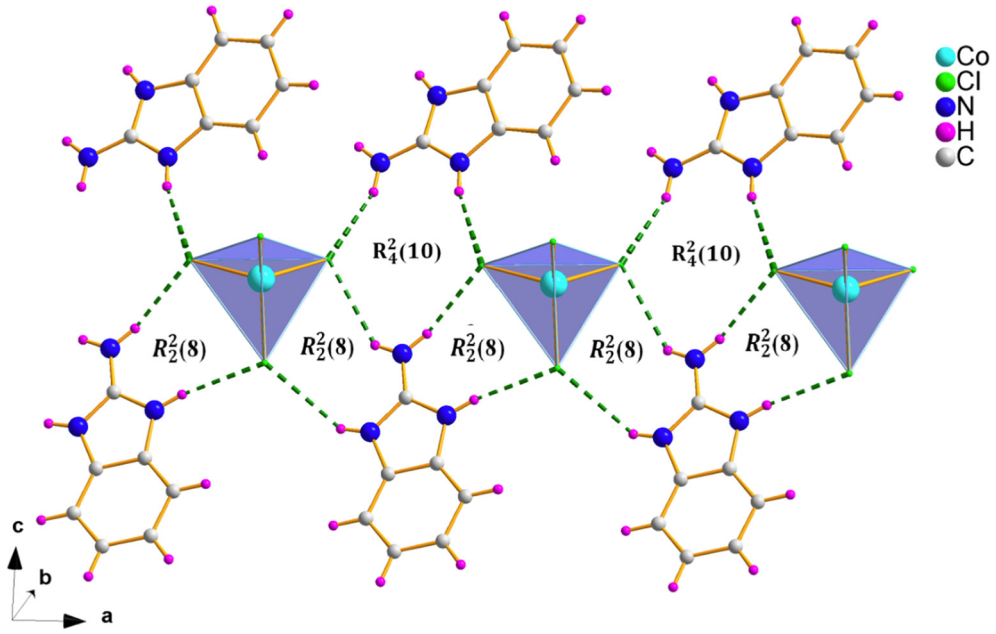


**Fig. 2.** View of the 1D supramolecular architecture of $(C_7H_8N_3)_2[CoCl_4]$ formed by hydrogen bonding interactions (hydrogen bonds are represented by dashed green lines).

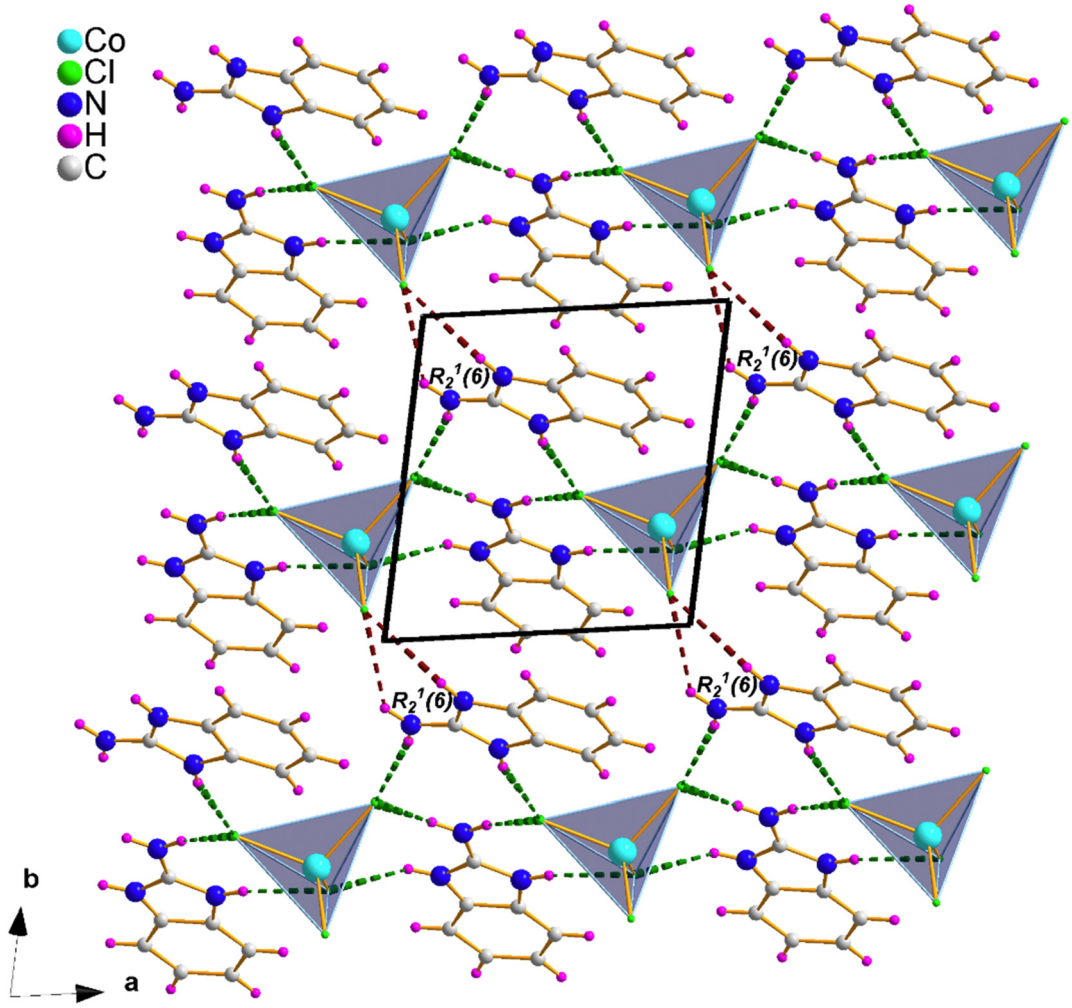


**Fig. 3.** View of the 2D supramolecular architecture layer of $(C_7H_8N_3)_2[CoCl_4]$formed by hydrogen bonding interactions (represented by dashed brown lines).

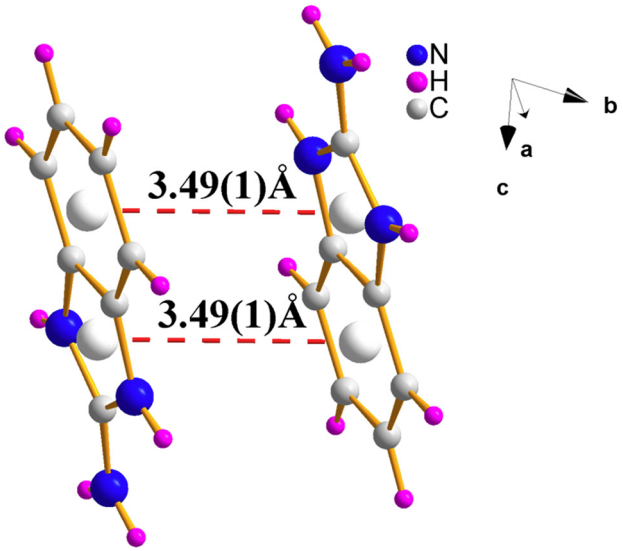


**Fig. 4.** The π-π stacking interactions formed by the organic parts, distance is measured between the centroids of opposite 5- and 6-membered rings.

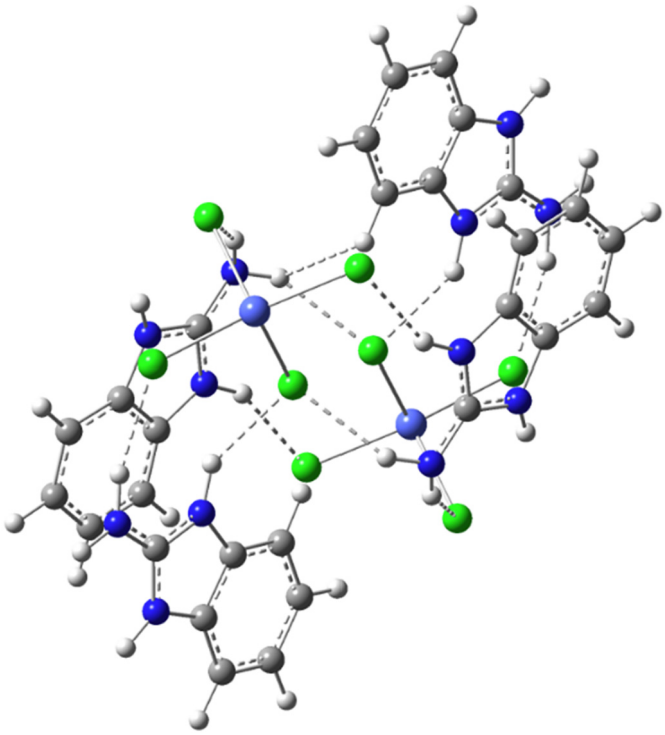

**Fig. 6.** The optimized geometry of the studied compound with the DFT/b3LYP Method.

### *3.4. Powder X-ray diffraction analysis*

In order to check the phase purity and homogeneity of the sample, powder X-ray diffraction (PXRD) patterns of the hybrid compound were also obtained at room temperature. As shown in Fig. 8, the peak positions of the experimental PXRD pattern are in agreement with the simulated ones from the crystal structure, indicating phase purity of the title compound. However, the difference in reflection intensities between the simulated and experimental patterns may be attributed to preferential orientation of the powder sample during collection of the experimental PXRD data.

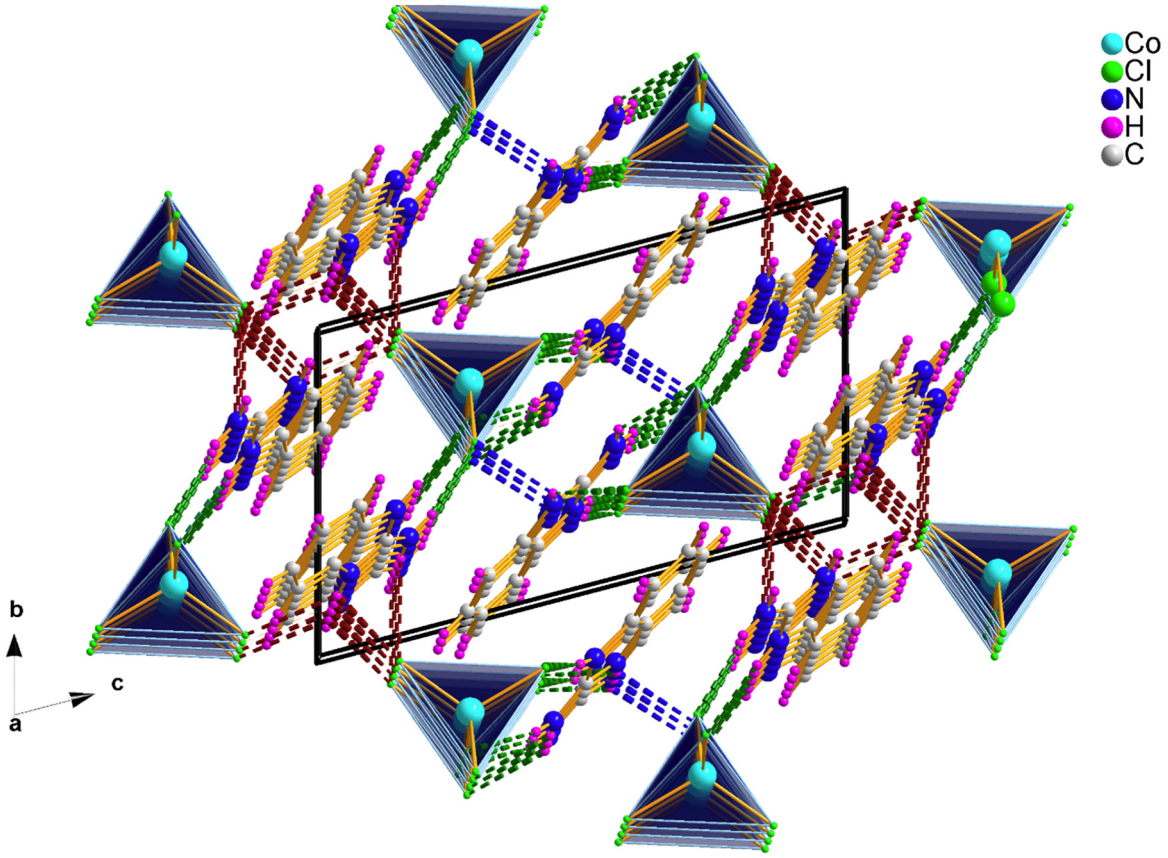


**Fig. 5.** Perspective view showing the 3D supramolecular architecture of $(C_7H_8N_3)_2[CoCl_4]$ formed by hydrogen bonding interactions (represented by dashed blue lines).

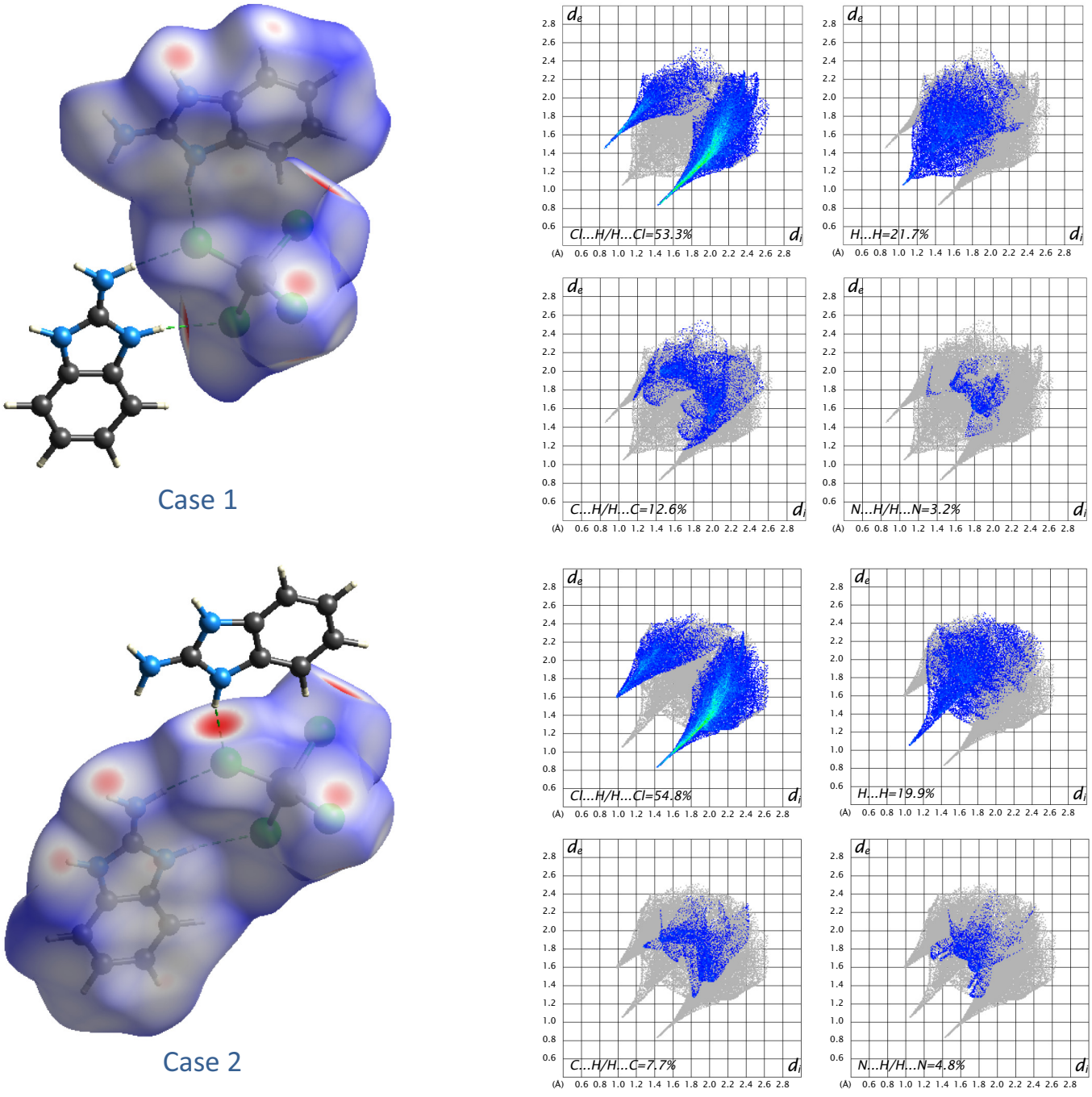


**Fig. 7.** 3D-Hirshfeld surface mapped over $d_{norm}$ and 2D fingerprint plots of the title compound resolved into Cl…H/H…Cl, H…H, C…H/H…C and N…H/H…N contacts showing the percentages participations to the total Hirshfeld surface area in two differents cases.

### *3.5. Infrared and Raman spectroscopy*

The experimental and calculated infrared spectra in the range of 4000–370 $cm^{-1}$ are shown in Fig. 9. The observed IR spectrum showed two strong bands at 3440 and 3320 $cm^{-1}$ assigned to the asymmetric and symmetric $NH_2$ stretching [34]. These two stretching bands were calculated at 3510 and 3390 $cm^{-1}$. The band observed at 3228 $cm^{-1}$ was attributed to the N—H stretching [34]; theoretically this stretching was found at 3254 $cm^{-1}$. The C—H vibration of the aromatic ring was observed at 3169 $cm^{-1}$ [35], the corresponding calculated value appears at 3190 $cm^{-1}$. The bands observed at 1687 and 1590 $cm^{-1}$ were attributed to the N—H bending and C═N stretching respectively [36]. However, these theoretical bands are located at 1713 and 1570 $cm^{-1}$. The bands observed at 1532 and 1480 $cm^{-1}$ were assigned to the C═C and C—N stretching respectively [37,38], theoretically these stretching were observed at 1513 and 1441 $cm^{-1}$. The in-plane aromatic C—H bending and rocking vibrations occur at 1060 and 760 $cm^{-1}$ [39]; the corresponding calculated values appear at 1080 and 745 $cm^{-1}$. The correlation graph of the experimental and theoretical vibrational frequencies for the title compound is shown in Fig. 10. The obtained correlation coefficient was equal to 0.991. As it can be seen from the correlation graph, the experimental frequencies were in good agreement with the calculated values. The shift differences observed between the experimental and calculated infrared spectra are due to the fact that

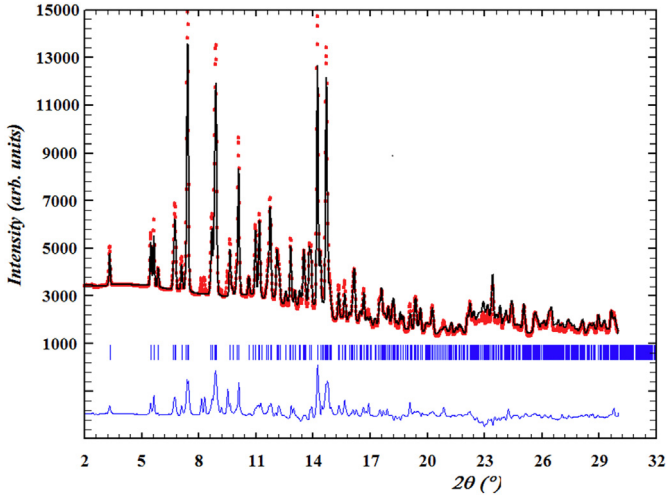


**Fig. 8.** Rietveld refinement of powder X-ray diffraction (PXRD) pattern of the title compound.

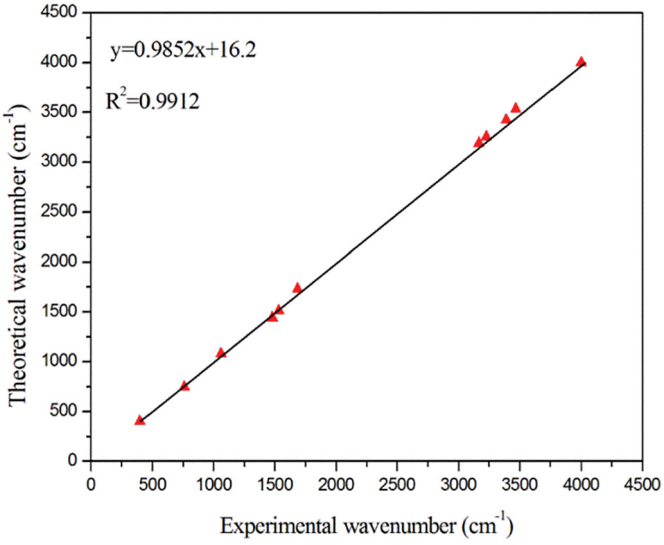


**Fig. 10.** The correlation graph of experimental and theoretical vibrational IR frequencies.

the DFT calculations of the vibrational frequency are performed for an isolated molecule while the intermolecular interaction with the neighboring molecule are absent, whereas the experimental spectrum are performed in the solid state when the weak interactions between the adjacent molecules could be taken.

The experimental and theoretical Raman spectra of the title compound recorded at room temperature are displayed in Fig. 11. Furthermore, the wavenumbers of the main bands and tentative assignments are provided in Table 4. The low frequency range 400–20 $cm^{-1}$ of the Raman spectra corresponds to the $[CoCl_4]^{2-}$ tetrahedra motion. In-plane and out-of-plane bending are assigned to the Raman peaks observed at 101 and 136 $cm^{-1}$ and calculated at 98 and 134 $cm^{-1}$ respectively. Their corresponding stretching vibrational modes are located at 256 and 348 $cm^{-1}$, respectively [40,41], the corresponding calculated value appears at 264 and 358 $cm^{-1}$.

### 3.6. Optical properties

#### 3.6.1. UV–vis absorption spectroscopy

The UV–vis absorption spectra of the title compound and 2-aminobenzimidazole were measured in an ethanol solution at room

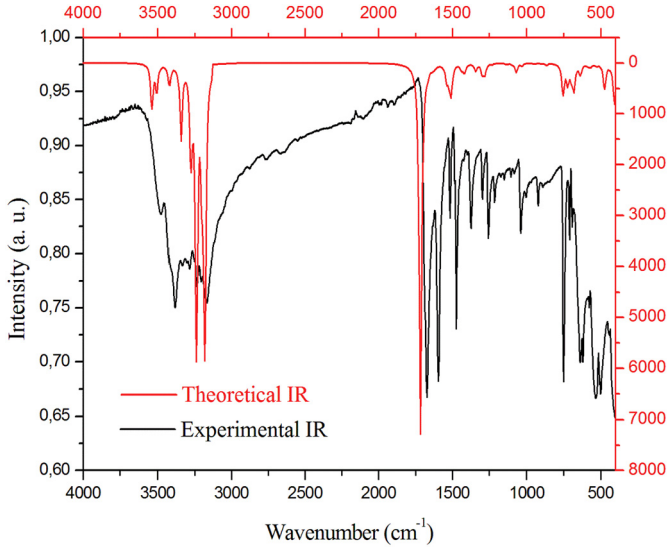


**Fig. 9.** The experimental and theoretical IR spectra of the title compound.

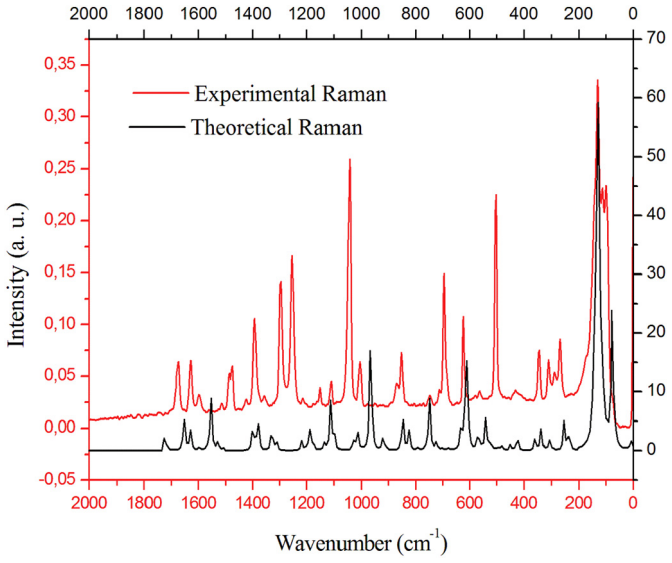


**Fig. 11.** The experimental and theoretical Raman spectra of the title compound.

**Table 4**
Experimental and theoretical infrared and Raman data for $(C_7H_8N_3)_2[CoCl_4]$.

| Exp IR ($cm^{-1}$) | Theo IR ($cm^{-1}$) | Exp Raman ($cm^{-1}$) | Theo Raman ($cm^{-1}$) | Assignment |
|---|---|---|---|---|
| 3440 | 3510 | – | – | $\overline{\nu}_{as}(NH_2)$ |
| 3320 | 3390 | – | – | $\overline{\nu}_{s}(NH_2)$ |
| 3228 | 3254 | – | – | $\overline{\nu}$(N–H) |
| 3169 | 3190 | – | – | $\overline{\nu}$(C–H) |
| 1687 | 1713 | 1672 | 1695 | δ($NH_2$) |
| 1590 | 1570 | 1592 | 1630 | $\overline{\nu}$(C=N) |
| 1532 | 1513 | 1520 | 1560 | $\overline{\nu}$(C–C) |
| 1480 | 1441 | 1477 | 1490 | $\overline{\nu}$(C–N) |
| 1060 | 1080 | 1051 | 1090 | δ(C–H) |
| 760 | 745 | 701 | 750 | ρ(C–H) |
| – | – | 348 | 358 | $\overline{\nu}_{as}$(Co–Cl) |
| – | – | 256 | 264 | $\overline{\nu}_{s}$(Co–Cl) |
| – | – | 136 | 134 | $\delta_{as}$(Cl-Co-Cl) |
| – | – | 101 | 98 | $\delta_{s}$(Cl-Co-Cl) |

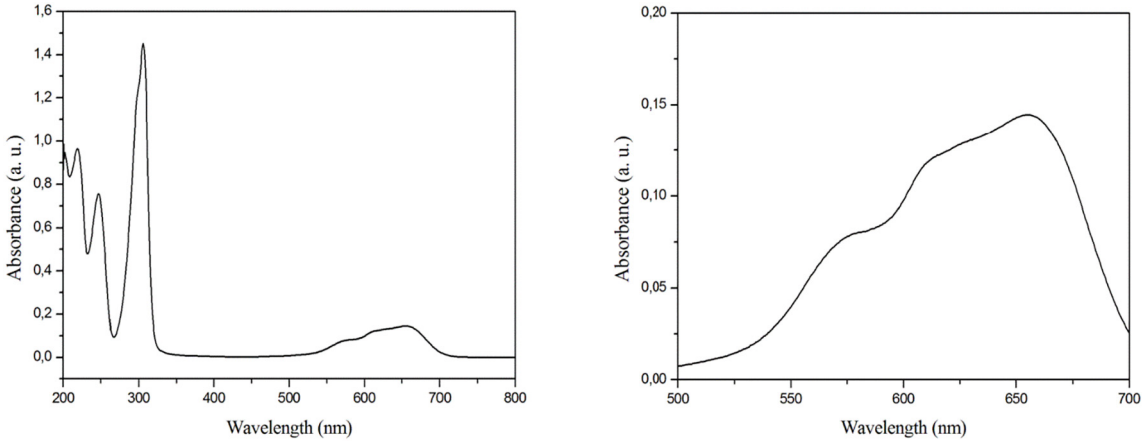


**Fig. 12.** Experimental UV–visible spectrum of $(C_7H_8N_3)_2[CoCl_4]$ (left) and zoom in the visible region (right).

temperature from 200 to 800 nm and are displayed in Figs. 12 and 13. The UV–vis absorption spectrum of the title compound shows the presence of three large and high intensity absorption bands in the UV region and some features with lower intensities at higher wavelengths. The absorption bands observed at 218, 245 and 303 nm are due to the $\pi \rightarrow \pi^*$ transitions of the organic part (Fig. 12). As can been observed, they are red shifted compared with the absorption bands of the 2-aminobenzimidazole which was located at 209, 235 and 291 nm (Fig. 13). The weak absorption bands observed at 609, 654 and 694 nm (Fig. 12) were attributed to the d-d electronic transitions $^4A_2(F) \rightarrow {}^4T_2(F)$, $^4A_2(F) \rightarrow {}^4T_1(F)$ and $^4A_2(F) \rightarrow {}^4T_1(P)$ that are typical of Co(II) coordination compounds.

*3.6.2. Optical band gap*

The absorption coefficient ($\alpha$) is a very important parameter for optical applications. The absorption coefficient ($\alpha$) is calculated by using the formula [42]:

$$\alpha = \frac{2.303 * A}{d}$$

where (A) is the absorbance and (d) is the thickness of the pellet (d = 1 cm).

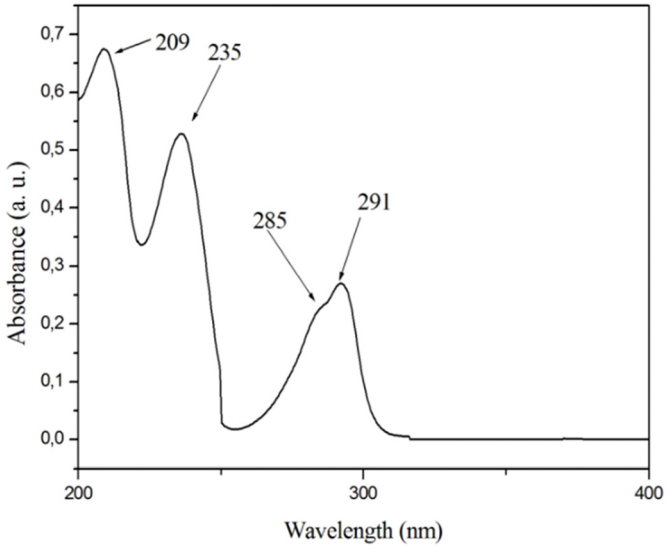


**Fig. 13.** Experimental UV–visible spectrum of 2-aminobenzimidazole.

The optical band gap ($E_g$) is related to absorption coefficient ($\alpha$) and photon energy ($h\nu$) through the Tauc relation [43]:

$$(\alpha h\nu) = B(h\nu - E_g)^n$$

where B is constant, $h\nu$ is the photon energy, $E_g$ is the optical band gap and n is the index, which takes different values depending on the mechanism of interband transitions $n = 2$ and $n = ½$ corresponding to indirect and direct transitions, respectively. Fig. 14 shows the variations of $(\alpha h\nu)^n$ versus the photon energy ($h\nu$) for different values of n. The $E_g$ value of the title compound was obtained by extrapolating the slope to $(\alpha h\nu)^n$ equal to zero. The obtained direct and indirect optical band gap values were 3.89 eV and 3.77 eV respectively. These band-gap values indicate that the title compound exhibits semiconductor behavior [44].

*3.6.3. Urbach energy*

In the low photon energy range ($h\nu < E_g$), absorption coefficient can be explained by Urbach relation [45]:

$$\alpha = \alpha_0 \exp\frac{h\nu}{E_u}$$

where $\alpha_0$ is a constant and $E_u$ is the Urbach energy which defines the width of the localized states in the band gap. $E_u$ is correlated to transitions between extended states of the valence band and localized states of the conduction band. The Urbach energy $E_u$ is obtained from the plot of $\ln(\alpha)$ versus photon energy ($h\nu$) which is deduced from the reciprocal of the slope of the linear part (Fig. 15). The $E_u$ value of the title compound is 3.25 eV.

*3.7. Thermal analysis and mass spectrometry*

Thermogravimetric analysis (TGA) and differential scanning calorimetry (DSC) experiments under argon atmosphere were carried out in order to determine the thermal stability of the studied compound. TGA and DSC methods were investigated in the temperature range 25–950 °C (Fig. 16). It is clear from the TGA curve that the compound decomposes in four weight loss stages. The first one lies in the temperature range of 100–140 °C related to the endothermic peak of the DSC curve. This can be assigned to the loss of some water molecules. This is confirmed by MS that reveals characteristic peaks of water during this step. The TGA experiment was performed in an argon glovebox were the crucibles were stored. The water concentration in the glovebox is below 0.1 ppm. It is very unlikely that the water molecule comes from the crucible or the instrument. The compound starts to decompose under argon at a temperature of 194.8 °C. The second and third steps of the TGA curve could be attributed to the decomposition of one of the organic moieties ($C_7H_8N_3$)

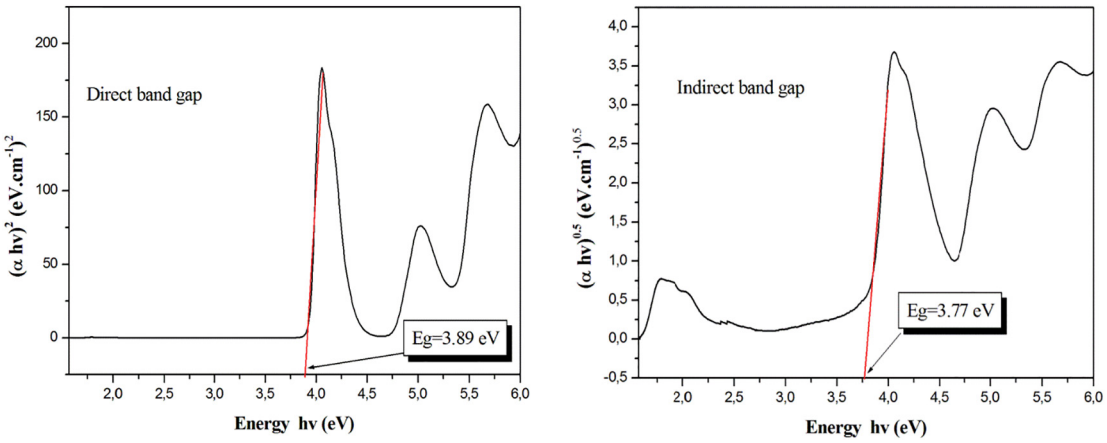


**Fig. 14.** Tauc Plots of $(\alpha h\nu)^2$ and $(\alpha h\nu)^{0.5}$ versus the photon energy ($h\nu$).

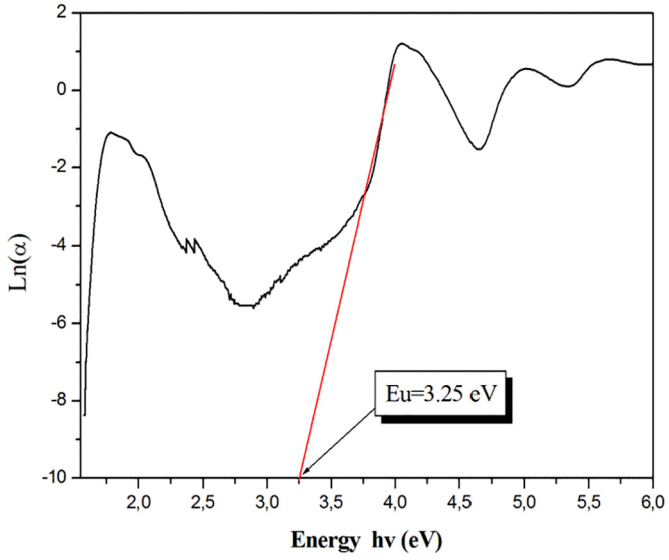


**Fig. 15.** Lnα versus hν (photon energy) of the title compound.

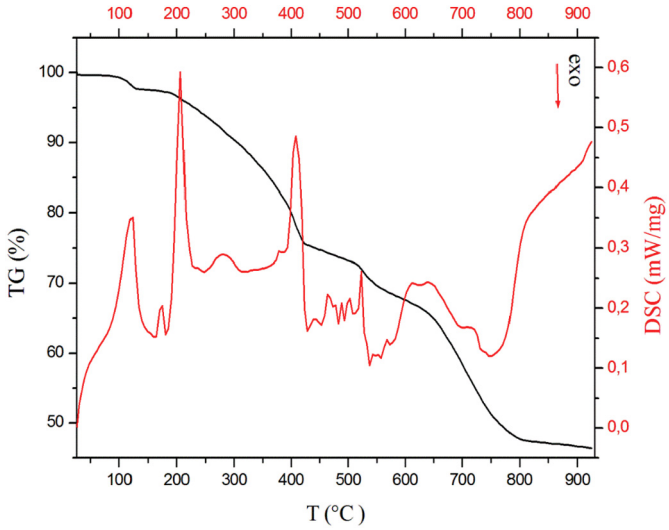


**Fig. 16.** The TGA-DSC thermograms of $(C_7H_8N_3)_2[CoCl_4]$ in the range of 25–950 °C.

(experimental weight loss: 28.6% and calculated weight loss is 29.4%). However, this decomposition occurs in multiple steps as indicated by the many DSC peaks in this region and the MS spectra did not allow to confirm the exact nature of the leaving fragments during this complex process (Fig. 17).

## 4. Conclusion

In summary, a new organic-inorganic hybrid compound, $(C_7H_8N_3)_2[CoCl_4]$, was synthesized by slow evaporation. It's crystal structure consists of a succession of mixed layers formed by organic cations and inorganic anions parallel to the (001) plane and propagate according to the *c*-axis. Layers further are assembled into a 3D supramolecular architecture through N-H···Cl hydrogen bonds and π···π interactions. The optimized geometry of the title compound using the B3LYP level of theory and X-ray diffraction structure show an excellent agreement between the experimental and calculated data. We found also that the theoretical values of infrared and Raman spectra are in good agreement with the experimental ones. The PXRD analysis confirms the phase purity of the crystalline sample. The tetrahedral environment of $Co^{2+}$ was confirmed by UV–visible spectroscopy. In addition, the direct (3.89 eV) and indirect (3.77 eV) optical band gap values were determined by Tauc method and show that this compound exhibits semiconductor behavior. Thermal analysis shows that the compound is stable up to 194.8 °C. Hirshfeld surface analysis confirmed that the structure is dominated by N-H…Cl interactions.

## CRediT authorship contribution statement

**S. Hassen:**Writing - original draft, Conceptualization, Data curation.**H. Chebbi:**Writing - original draft, Writing - review & editing, Methodology, Software, Validation.**Y. Arfaoui:**Visualization, Investigation, Software.**K. Robeyns:**Software, Validation, Writing - review & editing.**T. Steenhaut:** Writing - review & editing, Validation.**S. Hermans:**Writing - review & editing.**Y. Filinchuk:**Software, Validation, Writing - review & editing.

## Declaration of competing interest

The authors declare that they have no known competing financial interests or personal relationships that could have appeared to influence the work reported in this paper.

## Acknowledgements

Financial support from the Ministry of Higher Education and Scientific Research of Tunisia is gratefully acknowledged. The authors are

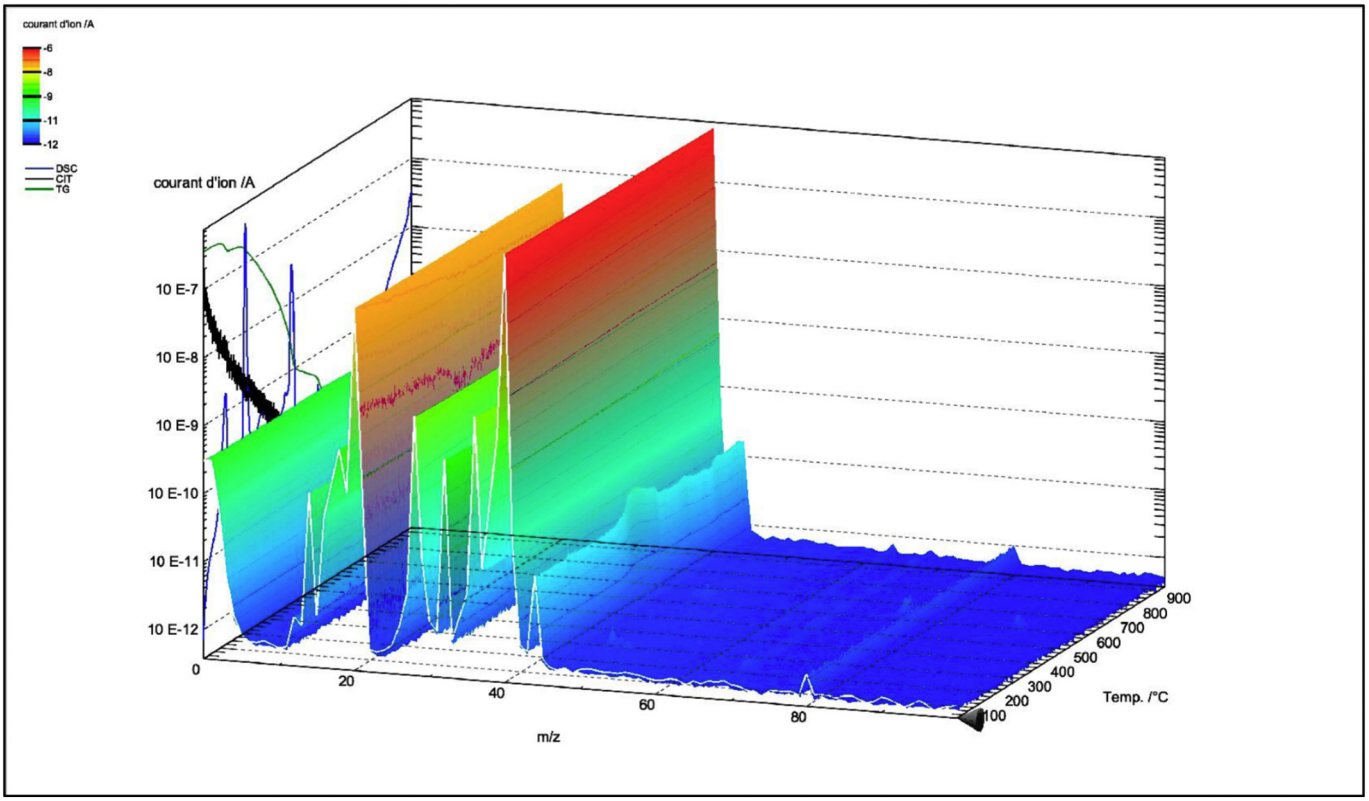


**Fig. 17.** Mass spectrometry coupled with TGA and DSC thermograms of $(C_7H_8N_3)_2[CoCl_4]$.

grateful to the ESRF for beamtime allocations, and SNBL staff for technical assistance. We thank FNRS for the FRIA fellowship for T.S. and the grants PDR T.0169.13, EQP U.N038.13 and U.N036.15 for funding.

## Appendix A. Supplementary data

Supplementary data to this article can be found online at https://doi.org/10.1016/j.saa.2020.118612.

## References

[1] N. Moutia, M. Ben Gzaiel, A. Oueslati, K. Khirouni, Electrical characterization and vibrational spectroscopic investigations of orderdisorder phase transitions in $[N(C_3H_7)_4]_2CoCl_4$ compound, J. Mol. Struct. 1134 (2017) 697–705, https://doi.org/10.1016/j.molstruc.2017.01.009.

[2] A. Abkari, I. Chaabane, K. Guidara, Dielectric properties and study of AC electrical conduction mechanisms by non-overlapping small polaron tunneling model in Bis (4-acetylanilinium) tetrachlorocuprate(II) compound, Phys. E. 83 (2016) 119–126, https://doi.org/10.1016/j.physe.2016.04.029.

[3] Y. Zheng, P. Yao-Qiong, F. Mei-Hua, S. Han, Z. Jia-Rong, L. Xiao-Ping Liu, Y. Le-Min Yang. N. Chun-Lin, Syntheses, crystal structures, and antibacterial activities of two tetrachlorocuprate(II) salts with substituted methyl pyridinium, Synth. React. Inorg. Met.-Org. Chem. 41 (2012) 839–844. doi:https://doi.org/10.1080/15533174.2011.591312.

[4] K. Azouzi, B. Hamdi, R. Zouari, A.B. Salah, Crystal structure, Hirshfeld surface analysis, vibrational properties, and electrical and dielectric studies of the bis (4-benzylpyridinium) tetrachlorocuprate (II), Ionics 22 (2016) 1669–1680, https://doi.org/10.1007/s11581-016-1697-y.

[5] N. Moutia, A. Oueslati, M.B. Gzaiel, K. Khirouni, Crystal structure and AC conductivity mechanism of $[N(C_3H_7)_4]_2CoCl_4$ compound, Phys. E. 83 (2016) 88–94, https://doi.org/10.1016/j.physe.2016.04.026.

[6] Y. Hui-Qing, L. De-Wei, M. Qian-Yi, C. Xiang-Xi, C. Qian-Yi, C. Yu, Z. Jia-Rong, N. Chun-Lin, Synthesis, three-dimensional network structure, weak interactions, and magnetic properties of Bis(quinolinium) tetrachlorocobaltate(II) dihydrate, J. Coord. Chem. 14 (2014) 1368–1372, https://doi.org/10.1080/15533174.2013.801864.

[7] A. Shapiro, C.P. Landee, M.M. Turnbull, J. Jornet, M. Deumal, J.J. Novoa, M.A. Robb, W. Lewis, Synthesis, structure, and magnetic properties of an antiferromagnetic spin-ladder complex: Bis(2,3-dimethylpyridinium) tetrabromocuprate, J. Am. Chem. Soc. 129 (2007) 952–959, https://doi.org/10.1021/ja066330m.

[8] A. Sen, S. Roy, S.C. Peter, A. Paul, U.V. Waghmare, S. Athinarayanan, Order-disorder structural phase transition and magnetocaloric effect in organic-inorganic halide hybrid $(C_2H_5NH_3)_2CoCl_4$, J. Solid State Chem. 258 (2018) 431–440, https://doi.org/10.1016/j.jssc.2017.10.036.

[9] A. Piecha-Bisiorek, A. Bienko, R. Jakubas, R. Boca, M.D. Weselski, V. Kinzhybalo, A. Pietraszko, M. Wojciechowska, W. Medycki, D. Kruk, Physical and structural characterization of imidazolium based organic-inorganic hybrid: $(C_3N_2H_5)_2[CoCl_4]$, J. Phys. Chem. A 120 (2016) 2014–2021, https://doi.org/10.1021/acs.jpca.5b11924.

[10] W. Amamou, N. Chniba-Boudjada, F. Zouari, Crystal structure, vibrational and magnetic properties of the monohydrated cobalt (II) complex with 1-(4-Nitrophenyl)-1H-imidazolium cation, $(C_9H_8N_3O_2)_2CoCl_4.H_2O$, J. Mol. Struct. 1127 (2017) 266–274. doi:https://doi.org/10.1016/j.molstruc.2016.07.111.

[11] A. Tounsi, B. Hamdi, R. Zouari, A. B. Salah, DFT(B3LYP/LanL2DZ), non-linear optical and electrical studies of a new hybrid compound: $[C_6H_{10}(NH_3)_2]CoCl_4.H_2O$, Phys. E 84 (2016) 384–394. doi:https://doi.org/10.1016/j.physe.2016.07.025.

[12] A. Abkari, I. Chaabane, K. Guidara, Synthesis, crystal structure, spectroscopic characterization and optical properties of bis(4-acetylanilinium) tetrachlorocobaltate(II), Phys. E. 86 (2017) 210–217, https://doi.org/10.1016/j.physe.2016.06.013.

[13] S. Chaouachi, S. Elleuch, B. Hamdi, R. Zouari, Experimental (FTIR, Raman, UV–visible and PL) and theoretical (DFT and TDDFT) studies on bis(8–hydroxyquinolinium) tetrachlorocobaltate(II) compound, J. Mol. Struct. 1125 (2016) 149–161, https://doi.org/10.1016/j.molstruc.2016.06.050.

[14] Y. Zheng, Z. Dong-Dong, Y. Lin-Liang, H. Song, Y. Le-Min, L. Xiao-Ping, Z. Jia-Rong, N. Chun-Lin, Syntheses, crystal structures and antibacterial properties of Bis(1-benzyl-4_-R-pyridinium) tetrabromocuprate(II) [R = $NH_2$ or $N(CH_3)_2$], Synth. React. Inorg. Met.-Org. Chem. 42 (2012) 238–245, https://doi.org/10.1080/15533174.2011.609853.

[15] C. Bejaoui, I. Ameur, N. Derbel, A. Linden, S. Abid, DFT calculations, crystal structure, Hirshfeld surface analyses and antibacterial studies of a new tetrachlorocuprate salt: $(C_6H_{16}N_2O)[CuCl_4]$, J. Mol. Struct. 1166 (2018) 7–14, https://doi.org/10.1016/j.molstruc.2018.04.003.

[16] M. Maha, D.E. Janzen, R. Mohamed, S. Wajda, Synthesis, crystal structure, thermal analysis, spectroscopic, and magnetic properties of a novel organic cation tetrachlorocobaltate(II), J. Supercond. Nov. Magn. 29 (2016) 1573–1581, https://doi.org/10.1007/s10948-016-3451-0.

[17] A. A. S, Nami, A. Husain, K. S. Siddiqi, B. L. Westcott, K. K. Vaughn, Synthesis, spectroscopic, magnetic and thermal properties of bimetallic salts, [Ni(L)][$MCl_4$] {where M= Co(II), Zn(II), Hg(II) and L = 3,7-bis(2-aminoethyl)-1,3,5,7-tetraazabicyclo (3.3.1)nonane}. X-ray structure of [Ni(L)][$CoCl_4$], Spectrochim. Acta.75A (2010) 444–447. doi:https://doi.org/10.1016/j.saa.2009.11.004.

[18] A. Kessentini, M. Belhouchet, J.J. Suñol, Y. Abid, T. Mhiri, Crystal structure, vibrational studies and optical properties of a new organic–inorganic hybrid compound $(C_{10}H_{28}N_4)CuCl_5Cl\text{-}4H_2O$, Spectrochim. Acta 134A (2015) 28–33https://doi.org/10.1016/j.saa.2014.06.073.

[19] A. Komasa, P. Barczyński, M.R. Sitarz, A. Katrusiak, Spectroscopic, structural and theoretical investigation of 1,3-bis(3-hydroxymethylpyridinium)propane dibromide, tetrabromozincate and tetrabromocuprate, J. Mol. Struct. 1163 (2018) 345–356, https://doi.org/10.1016/j.molstruc.2018.03.001.
[20] L.J. Farrugia, *WinGX* and *ORTEP for Windows*: an update, J. Appl. Crystallogr. 32 (1999) 837–838, https://doi.org/10.1107/S0021889812029111.
[21] G.M. Sheldrick, SHELXS-97, Program for Crystal Structure Solution, University of Göttingen, Germany, 1997.
[22] G.M. Sheldrick, SHELXL-2014, Program for the Refinement of Crystal Structures University of Göttingen, Göttingen, Germany, 2014.
[23] Gaussian 09, Revision A.1, M. J. Frisch, G. W. Trucks, H. B. Schlegel, G. E. Scuseria, M. A. Robb, J. R. Cheeseman, G. Scalmani, V. Barone, B. Mennucci, G. A. Petersson, H. Nakatsuji, M. Caricato, X. Li, H. P. Hratchian, A. F. Izmaylov, J. Bloino, G. Zheng, J. L. Sonnenberg, M. Hada, M. Ehara, K. Toyota, R. Fukuda, J. Hasegawa, M. Ishida, T. Nakajima, Y. Honda, O. Kitao, H. Nakai, T. Vreven, J. A. Montgomery, Jr., J. E. Peralta, F. Ogliaro, M. Bearpark, J. J. Heyd, E. Brothers, K. N. Kudin, V. N. Staroverov, R. Kobayashi, J. Normand, K. Raghavachari, A. Rendell, J. C. Burant, S. S. Iyengar, J. Tomasi, M. Cossi, N. Rega, J. M. Millam, M. Klene, J. E. Knox, J. B. Cross, V. Bakken, C. Adamo, J. Jaramillo, R. Gomperts, R. E. Stratmann, O. Yazyev, A. J. Austin, R. Cammi, C. Pomelli, J. W. Ochterski, R. L. Martin, K. Morokuma, V. G. Zakrzewski, G. A. Voth, P. Salvador, J. J. Dannenberg, S. Dapprich, A. D. Daniels, O. Farkas, J. B. Foresman, J. V. Ortiz, J. Cioslowski, and D. J. Fox, Gaussian, Inc., Wallingford CT, 2009.
[24] R G. Parr, W. Yang, Density Functional Theory of Atoms and Molecules Oxford University Press, Oxford, 1989.
[25] R. Krishnan, J. S. Binkley, R. Seeger, J. A. Pople, Self-consistent molecular orbital methods. XX. A basis set for correlated wave functions, J. Chem. phys.72 (1980) 650. doi:https://doi.org/10.1063/1.438955.
[26] S.K. Wolff, D.J. Greenwood, J.J. McKinnon, D. Jayatilaka, M.A. Spackman, Crystal Explorer, 2012.
[27] M. Mghandef, H. Boughzala, Crystal structure of bis(2-amino-5-chloropyridinium) tetrachloridocobaltate(II), Acta Cryst E71 (2015) 555–557, https://doi.org/10.1107/S2056989015007707.
[28] M. Mghandef, H. Boughzala, 1-(4-Hydroxyphenyl) piperazine-1, 4-diium tetrachloridocobalt(II) monohydrate, Acta Cryst E70 (2014) 75, https://doi.org/10.1107/S1600536814001767.
[29] O.B. Moussa, H. Chebbi, M.F. Zid, Synthesis, crystal structure, vibrational study, optical properties and Hirshfeld surface analysis of bis(2,6-diaminopyridinium) tetrachloridocobaltate(II) monohydrate, J. Mol. Struct. 1180 (2019) 72–80, https://doi.org/10.1016/j.molstruc.2018.11.077.
[30] H. Kaikai, D. Bowen, J. Shouwen Jin, D. Aihua, J. Shide, Z. Jin Zhu, Z. Huan, W. Daqi, Syntheses and structure characterization of ten acid-base hybrid crystals based on imidazole derivatives and mineral acids, J. Mol. Struct. 1157 (2018) 247–262, https://doi.org/10.1016/j.molstruc.2017.12.041.
[31] S. Choubey, S. Roy, K. Bhar, P. Mitra, J. Ribas, B.K. Ghosh, Varied dicarboxylate bridges in dinuclear trigonal prismatic manganese(II) and octahedral nickel(II) compounds containing tetradentate N-donor Schiff bases: syntheses, structures and magnetic behaviors, Polyhedron 74 (2014) 134–143, https://doi.org/10.1016/j.poly.2014.01.024.
[32] G.J. Perpétuo, J. Janczak, Supramolecular hydrogen-bonding networks in the 1-(diaminomethylenene) thiouron-1-ium 4-hydroxybenzoate, 3, 4-dihydroxybenzoate and 3,4,5-trihydroxybenzoate monohydrate crystals, J. Mol. Struct. 1041 (2013) 127–138, https://doi.org/10.1016/j.molstruc.2013.03.015.
[33] E. Pahonţu, D.C. Ilieş, S. Shova, C. Paraschivescu, M. Badea, A. Gulea, T. Roşu, Synthesis, characterization, crystal structure and antimicrobial activity of copper(II) complexes with the Schiff Base derived from 2-Hydroxy-4-methoxybenzaldehyde, Molecules 20 (2015) 5771–5792, https://doi.org/10.3390/molecules20045771.
[34] S. Sudha, M. Karabacak, M. Kurt, M. Cinar, N. Sundaraganesan, Molecular structure, vibrational spectroscopic, first-order hyperpolarizability and HOMO, LUMO studies of 2-aminobenzimidazole, Spectrochim. Acta 84A (2011) 184–195, https://doi.org/10.1016/j.saa.2011.09.028.
[35] A. A. S. Nami, A. Husain, K. S. Siddiqi, B. L. Westcott, K. Kopp-Vaughn, Synthesis, spectroscopic, magnetic and thermal properties of bimetallic salts, [Ni(L)][MCl4] {where M= Co(II), Zn(II), Hg(II) and L = 3,7-bis(2-aminoethyl)-1,3,5,7-tetraazabicyclo(3.3.1)nonane}. X-ray structure of [Ni (L)][CoCl4], Spectrochim. Acta 75A (2010) 444–447. doi:https://doi.org/10.1016/j.saa.2009.11.004.
[36] M.M. Abo-Aly, A.M. Salem, M.A. Sayed, A.A. Abdel Aziz, Spectroscopic and structural studies of the Schiff base 3-methoxy-N-salicylidene-o-amino phenol complexes with some transition metal ions and their antibacterial, antifungal activities, Spectrochim. Acta 136A (2015) 993–1000, https://doi.org/10.1016/j.saa.2014.09.122.
[37] K. Ahmad, A. Al-Nasr, R.M. Ramadan, Spectroscopic studies and biological activity of some transition metal complexes of unusual Schiff base, Spectrochim. Acta 105A (2013) 14–19, https://doi.org/10.1016/j.saa.2012.12.008.
[38] S. Hassen, H. Chebbi, M.F. Zid, Y. Arfaoui, Crystal structure, spectroscopic study, photoluminescent properties and DFT calculations of the 2-guanidinobenzimidazolium dichloride and dibromide monohydrate salts, J. Mol. Struct. 1167 (2018) 1–10, https://doi.org/10.1016/j.molstruc.2018.04.073.
[39] N. Ennaceur, R. Henchiri, B. Jalel, M. Cordier, I. Ledoux-Rak, E. Elaloui, Synthesis, crystal structure, and spectroscopic characterization supported by DFT calculations of organoarsenic compound, J. Mol. Struct. 1144 (2017) 25–32, https://doi.org/10.1016/j.molstruc.2017.05.007.
[40] M.A. Kandhaswamy, V. Srinivasan, Synthesis and characterization of tetraethylammonium tetrachlorocobaltate crystals, Bull. Mater. Sci. 25 (2002) 41–45, https://doi.org/10.1007/BF02704593.
[41] A. Wesełucha-Birczyn'ska, C. Paluszkiewicz, Analysis of tetrachlorocuprate(II) and tetrachlorocobaltate(II) anion vibrations in their compounds with cinchonine. FT-IR and Raman study, J. Mol. Struct. 614 (2002) 339–343. doi:https://doi.org/10.1016/S0022-2860(02)00274-0.
[42] A. Eshaghi, A. Graeli, Optical and electrical properties of indium tin oxide (ITO) nanostructured thin films deposited on polycarbonate substrates "thickness effect", Optik Int. J. Light Electron Opt. 125 (2014) 1478–1481, https://doi.org/10.1016/j.ijleo.2013.09.011.
[43] A. Ayeshamariam, S. Ramalingam, M. Bououdina, M. Jayachandran, Preparation and characterizations of SnO2 nanopowder and spectroscopic (FTIR, FT-Raman, UV-visible and NMR) analysis using HF and DFT calculations, Spectrochim. Acta. Part A: Molecular and Biomolecular Spectroscopy 118A (2014) 1135–1143, https://doi.org/10.1016/j.saa.2013.09.030.
[44] E. Rosencher, B. Vinter, Optoelectronics, Cambridge University Press, 2002.
[45] M.S. Shakeri, M. Rezvani, Optical band gap and spectroscopic study of lithium alumino silicate glass containing $Y^{3+}$ ions, Spectrochim. Acta 79A (2011) 1920–1925, https://doi.org/10.1016/j.saa.2011.05.090.